공학석사 학위논문

Simple Synthesis of Urchin-like Pt-Ni Bimetallic Nanostructures for Oxygen Reduction Reaction Electrocatalyst Application

성게모양의 백금-니켈 나노구조의 합성과 산소 환원 반응 전기화학 촉매로의 이용

2015년 8 월

서울대학교 대학원

화학생물공학부

서 필 선

Simple Synthesis of Urchin-like Pt-Ni Bimetallic Nanostructures for Oxygen Reduction Reaction Electrocatalyst Application

지도 교수 현 택 환

이 논문을 공학석사 학위논문으로 제출함

2015 년 6 월

서울대학교 대학원

화학생물공학부

서 필 선

서필선의 공학석사 학위논문을 인준함

2015 년 6 월

위 원 장 _____ (인)

부위원장 _____ (인)

위 원 _____ (인)

Abstract

Simple Synthesis of Urchin-like Pt-Ni Bimetallic Nanostructures for Oxygen Reduction Reaction Electrocatalyst Application

Pilseon Seo

School of Chemical and Biological Engineering

The Graduate School

Seoul National University

Proton exchange membrane fuel cells (PEMFCs) are considered as one of the most promising environmentally friendly energy technologies to produce electricity. In PEMFCs, the most important reaction is oxygen reduction reaction (ORR) at cathode. Pt metal is widely used as electrocatalyst for ORR in commercial fuel cells. However, its practical use is limited by high cost because Pt is an element hardly found on the Earth crust. A high-activity

electrocatalyst accelerating the ORR reaction must be developed to commercialize PEMFCs as ORR is the bottleneck in the overall reactions. Among many ORR electrocatalysts reported so far, Pt-Ni alloy is known as a promising candidate for high-activity catalyst materials because of its low cost and enhanced activity compared to Pt. Various nanostructures of the Pt-Ni alloy materials have been tested as ORR electrocatalysts to increase the surface to volume ratio and to enhance catalytic performance. Herein we synthesized urchin-like Pt-Ni bimetallic nanostructures by a simple heat-up method. Alloy composition was adjusted by varying the molar ratio of precursors. These urchin-like Pt-Ni bimetallic nanostructures showed higher catalytic activity in ORR than the commercial Pt catalyst.

Keywords: Oxygen reduction reaction, Proton exchange membrane fuel cells, urchin-like nanostructure, electrocatalyst, Pt-Ni alloy

Student Number: 2012-23266

Contents

List of Tables

List of Figures

Chapter 1 Introduction

Many alternative energy resources are strudied to tackle the various problems of fossil fuels. Fuel cell is one of the promising energy technologies because it does not produce pollutants during the whole operation process. Many types of fuel cells have been developed. The proton exchange membrane fuel cell (PEMFC) has many advantages. For example, it operates at low temperature and under normal pressure, and has high power density.[1] PEMFC is expected to be applied for transportation, stationary fuel cells and portable fuel cells. For PEMFC, the oxygen reduction reaction (ORR) at the cathode is the most important reaction. Because ORR is a sluggish reaction, platinum group metal (PGM)-based materials are often used to catalyze ORR. However, high price of PGM and its lack of reserves are considered as demerits. Many efforts have been made (1) to raise the performance of PGM catalysts and (2) to develop a new, cheap, and efficient non-PGM catalyst. As for the first approach, alloy nanostructures of Pt and transition metal can be a good candidate for high-performance catalysts with less PGM content.[3] The electronic structure, surface orientation, and morphology of electrocatalysts are known as important factors in efficient catalysis.[4]

The following chapters describe the principles of PEMFCs and ORR, and overviews of other researches on ORR electrocatalyst, especially on PtNi bimetallic nanostructure.

1.1 Introduction of Proton Exchange Membrane Fuel Cells

Fuel cells can convert chemical energy of fuels into electrical power. The first report of fuel cells was in 1839.[5] Until now five types of fuel cells, based on the electrolyte, have been developed, alkaline fuel cell (AFC), proton exchange membrane fuel cell (PEMFC), phosphoric acid fuel cell (PAFC), molten carbonate fuel cell (MCFC), and solid oxide fuel cell (SOFC).[6](Fig. 1.1) Their electrical efficiencies are almost 40-60 percent.

At the anode (+), the oxidation reaction takes place and electrons are extracted. Electrons travel the external load toward the cathode (-), producing electrical energy. The electrons take part in reduction reaction at the cathode (-). Among the five types of fuel cells, PEMFC is the most studied one because it has high power density and operates under mild environment. In the case of PEMFCs, the anode reaction is $H_2 = 2H^+ + 2e^-$, and the cathode reaction is $1/2O_2 + 2H^+ + 2e^- = H_2O$, called oxygen reduction reaction (ORR). The overall reaction is

shown below.

$H_2 + 1/2O_2 = H_2O$ $E^o = 1.229V$ (vs. SHE)

Nafion, a sulfonated tetrafluoroethylene based fluoropolymer-copolymer, is a representative electrolyte that effectively conducts H^+ ions only.

The electrolyte, gaseous reactants, electrocatalyst and current collector must be in close contact (this area is named the triple-phase-boundary interface), so that the reactions would occur efficiently. The ORR is a slow four-electron reaction, and the whole reaction rate is limited by ORR. Many researchers have tried to enhance the activity of ORR electrocatalysts and to improve the overall efficiency.

1.2 Electrocatalysts for Oxygen Reduction Reaction (ORR)

It is known that platinum (Pt) is the most active catalytic material for ORR if fuel cells operate in pure hydrogen and air.[6] Until now, although researchers made a lot of effort to develop non-noble metal electrocatalysts for ORR, there are few results about non-noble metal materials that show higher activity than Pt. However, the cost of Pt is too high to be commercialized. Also the reserves of Pt is too low, and its lifetime in fuel cells is not long enough to operate in real system.

Both reducing the content of Pt and enhancing activity and lifetime of electrocatalysts are probable approaches to lower the cost.

Because ORR occurs on the surface of the electrocatalyst, making nanostructures can increase the surface-to-volume ratio. In the 1960s, electrocatalysts of Pt nanoparticles on the carbon support were developed to reduce Pt content. The performance and lifetime were not compromised compared to the previous bulk-type catalysts.[7] Some research papers proved that the shape control of nanostructures can also increase the number of active sites on Pt nanoparticles such as nanorods, nanocubes, and nanodendrites.[8] Another trend is using alloy of PGM and transition metal as a electrocatalyst and is described in next chapter.[9]

1.3 Pt-Ni bimetallic nanoparticles as ORR Electrocatalysts

Many density functional theory (DFT) calculation results predicted that making alloy of Pt and transition metal can alter the electronic structure of Pt,[10] which can affect adsorption energies and desorption energies of oxygen species including molecular oxygen (reactant), intermediate products and final product on the surface of electrocatalysts.

Stamenkovic *et al.* conducted DFT calculations and experimentally investigated the activity of Pt-3d transition metal alloy for ORR and demonstrated that Pt-Ni bimetallic alloy is one of the promising candidates as ORR electrocatalysts.[10(a)](Fig. 1.2) Various types of Pt-Ni bimetallic alloy nanoparticles such as octahedra[3a], truncated octahedra,[3b] cube, [4] and icosahedra[3c] were synthesized and studied. Especially Zhang synthesized Pt_3Ni nanoctahedra and nanocubes enclosed by {111} and {100} facets respectively and investigated the shape dependence of ORR activity.[4] Stamenkovic also found that Pt_3Ni {111} is one of the most active surfaces.[9a] (Fig. 1.3)

Recently, the urchin-like dendritic structure for ORR electrocatalyst has attracted attention because of its large surface area and rough surfae for adsorption sites.[11,12,13] Although recent advancements have been made in the synthesis of Pt-Ni bimetallic nanoparticles with different morphologies, controlling the shape and composition of Pt-Ni bimetallic nanoparticles is challenging. Herein, we report the facile one-pot synthesis of urchin-like Pt-Ni nanostructures by utilizing a simple heat-up method.

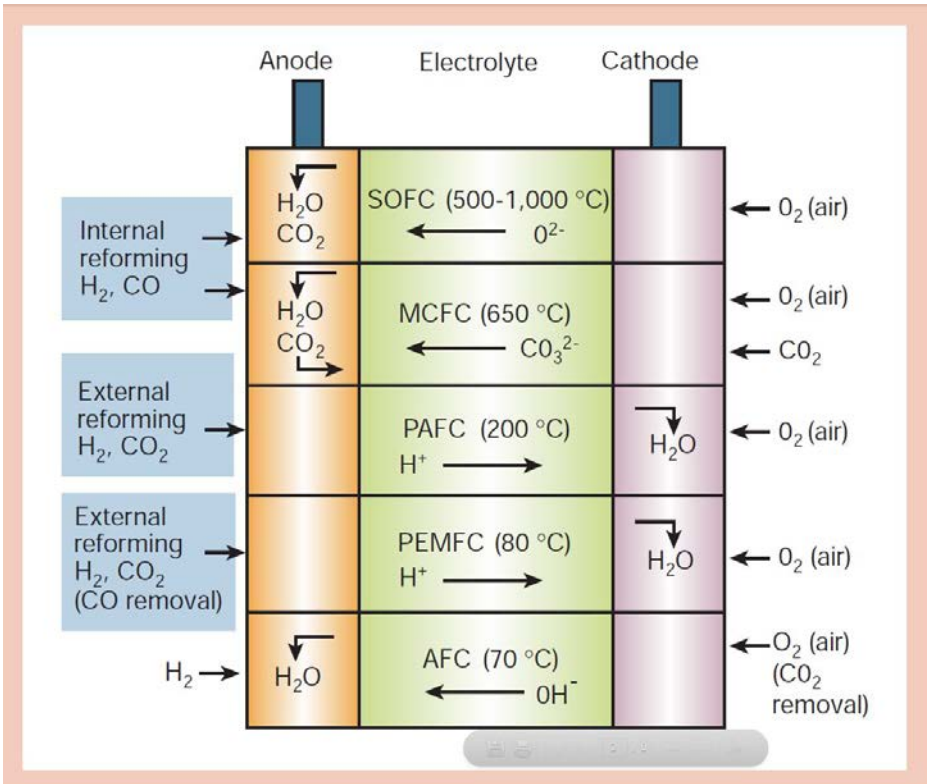

Figure 1.1 Summary of fuel cell types. (from Ref. 6 Brian C. H. Steele, Angelika Heinzel, *Nature* 2001, 414, 345-352.)

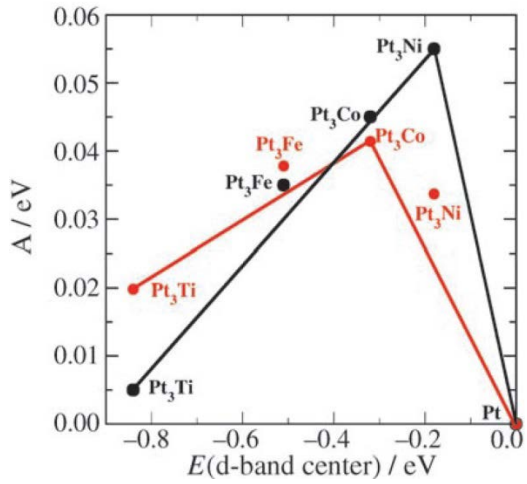

Figure 1.2 Activity versus the experimentally measured d-band center position at 0.9V relative to platinum. The activity predicted from DFT simulations is shown in black, and the measured activity is shown in red. (from Ref. 10 *(a)* V. Stamenkovic, B. S. Mun, K. J. J. Mayrhofer, P. N. Ross, N. M Markovic, J. Rossmeisl, J. Greeley and J. K. Nørskov, *Angew. Chem., Int. Ed*, 2006, **45**, 2897-2901.)

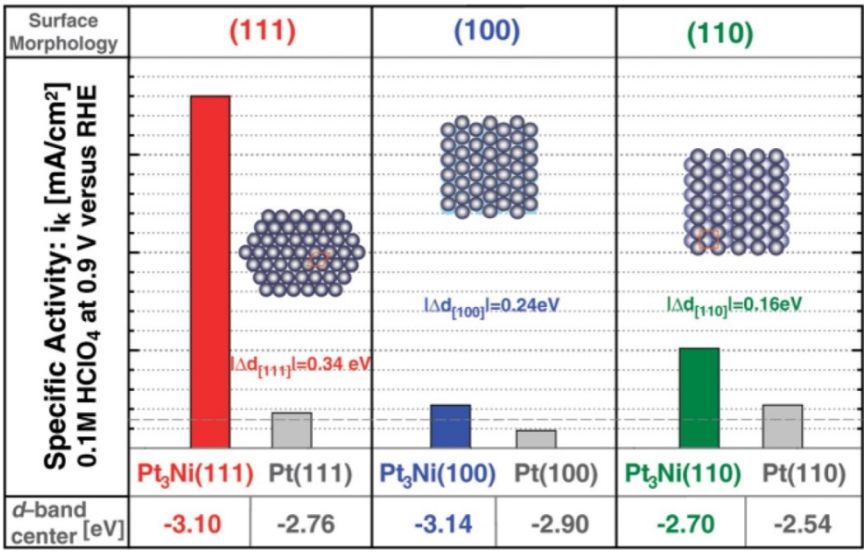

Figure 1.3 Influence of the surface morphology and electronic surface properties on the kinetics of ORR. (from Ref. 9(*a*) V. R. Stamenkovic, B. Fowler, B. S. Mun, G. Wang, P. N. Ross, C. A. Lucas and N. M. Markovic, *Science*, 2007, 315, 493-497.)

Chapter 2 Experiments

2.1 Chemicals

Benzyl ether, hexadecylamine, 1-adamantane carboxylic acid, and nickel acetylacetonate ($Ni(acac)_2$) were purchased from Aldrich Chemical Co. Platinum acetylacetonate ($Pt(acac)_2$) was purchased from Strem. These chemicals were used without further purification.

2.2 Synthesis of the urchin-like Pt-Ni bimetallic nanostructures

The urchin-like Pt-Ni nanostructures were synthesized from a mixture solution containing $Pt(acac)_2$, $Ni(acac)_2$, hexadecylamine, and 1-adamantane carboxylic acid by the heat-up process. In a typical synthesis for Pt_2Ni nanostructures, 50 mg of $Pt(acac)_2$ (0.13 mmol), 17 mg of $Ni(acac)_2$ (0.065 mmol), 1g of hexadecylamine (4.14 mmol), and 0.144 g of 1-adamantane carboxylic acid (0.8 mmol) were dissolved in 10 ml of benzyl ether and the reaction mixture was degassed under vacuum for 1 hour. Then, under Ar atmosphere, the mixture solution was heated up to 240 ^oC at the heating rate of 4 ^oC/min and then kept at the same temperature for 15 min. After the

vessel cooled down, the mixture solution was washed by adding ethanol. After washing that twice, the products were dispersed in an organic solvent such as hexane and chloroform. To synthesize Pt_3Ni and PtNi nanostructures, 11 mg and 33 mg of $Ni(acac)_2$ were added respectively, and the other conditions were the same.

2.3 Characterization

All the transmission electron microscopy (TEM) and the high-resolution TEM (HRTEM) images were obtained on a JEOL EM-2010 and Tecnai F-20 microscope at an accelerating voltage of 200 kV. Energy-filtered TEM (EF-TEM) and HRTEM were measured by JEOL-2200FS equipped with the image Cs corrector. The powder X-ray diffraction (XRD) patterns were obtained by a Rigaku D/Max-3C diffractometer (Cu Kα radiation, λ = 0.15418 nm). The elemental analysis was performed by inductively coupled plasma atomic emission spectroscopy (ICP-AES) and by an ICPS-7500 spectrometer (Shimadzu). The X-ray absorption fine structure (XAFS) data of the Pt L_{III} edge were obtained by 7D beamline at the Pohang Light Source (PLS).

2.4 Electrochemical measurements

Urchin-like Pt-Ni nanostructures with the three molar ratios of Pt to Ni (1:1, 2:1, and 3:1) were loaded onto carbon supports (Vulcan XC-72) via hexane solution at a weight ratio of 20% Pt-Ni bimetallic nanostructures to 80% carbon support. The Pt-Ni bimetallic nanostructures were added to 300 ml of hexane, sonicated for 2 hrs, and stirred overnight. The Pt-Ni loading and atomic composition ratio on the carbon support was measured by TGA analysis (TA5000/SDT Q600). The electrochemical characteristics and oxygen reduction activity of the urchin-like Pt-Ni nanostructures and commercial Pt (20 wt%; J.M.) were obtained by cyclic voltammetry (CV) and rotating disk electrode (RDE) measurements in a 0.1 M $HClO_4$ solution and a 0.5 M H_2SO_4 solution. Electrochemical measurements were conducted in an Autolab potentiostat (PGSTA101) using a conventional three-electrode electrochemical cell comprised of a platinum wire counter electrode, saturated calomel reference electrode (SCE), and glassy carbon (GC,) RDE working electrode at ambient temperature. The CV was acquired in the potential range from 0.05 to 1.00 V vs. RHE at a scan rate of 20 mV s^{-1}. ORR polarization curves were obtained by a RDE at 1,600 rpm, with scanning potential ranging from 0.05 to 1.05 V vs. RHE at a scan rate of 10 mV s^{-1} in 0.1 M $HClO_4$ under an O_2

flow. To confirm the surface structure of nanoparticle, CV was measured 0.5 M H_2SO_4 under Ar.

Chapter 3 Result and discussion

Here, we report the facile one-pot synthesis of urchin-like Pt-Ni bimetallic nanostructures. The schematic diagrams of the synthesis is shown in Fig. 3.1. And the transmission electron microscopy (TEM) images of the products are shown in Fig. 3.2. We can synthesize Pt_xNi (x=1, 2, 3) by varying the molar ratio of precursors. To confirm the distribution of Pt and Ni metal in the nanostructures, we performed the energy-filtered TEM (EF-TEM) elemental mapping analysis. The results show an even distribution of Pt and Ni elements throughout the entire nanostructures. The final compositions of the nanostructures are identified by inductively coupled plasma atomic emission spectrometry (ICP-AES), shown Table 3.1. All the peaks in the X-ray diffraction (XRD) patterns shown in Fig. 3.3 can be assigned to the (111), (200), and (220) lattice planes of a face-centered cubic (fcc) phase. There was no characteristic peak for nickel or oxide species. As Ni composition in nanostructures increases, the (111) peak shifts toward upper angle, which means the lattice constant decreases by the formation of Pt-Ni alloys.

To understand the formation mechanism, we did controlled experiments by varying the experimental factors, for example, heating rates, reaction temperature, and concentrations of surfactants and precursors. When we used only $Ni(acac)_2$ as the precursor, there was no particles. While, when we used only $Pt(acac)_2$ as the precursor, we were able to obtain truncated Pt nanoparticles of which size is about 30 nm. (Fig. 3.4) It indicates that $Ni(acac)_2$ is more difficult to be decomposed than $Pt(acac)_2$ and the urchin-like nanostructures can be synthesized by adding $Pt(acac)_2$ and $(acac)_2$ simultaneously. We also can deduce that $Ni(acac)_2$ is needed to control the morphology to form the urchin-like nanostructures in the synthesis, which supports the previous report.[11] Next, we changed the heating rate, higher and lower than 4 ^oC/min, and each rate was 2 ^oC/min and 6 ^oC/min. The reaction products were irregular multipod-shaped nanostructures. (Fig. 3.5 (a) and (b)) It means that there is an optimal heating rate to get the nanostructures with good shapes. We also performed controlled experiments at temperature, higher and lower than 240 ^oC. (Fig. 3.5 (c) and (d)) When the nanostructures were made at 200 ^oC, the shape was truncated and not uniform, while at 260 ^oC, the mixture of two kinds of nanoparticles was obtained. When hexadecylamine or 1-adamantanecarboxylic acid was used as the only surfactant,

aggregates containing spherical nanoparticles were produced. (Fig. 3.5 (e) and (f)) It's because the growth rate couldn't be controlled successfully. So, the combination of two different kinds of surfactants is important to control the growth rate of nanostructures, and it coincides with the previous studies. [3(b), 14]

We took the aliquot samples at various stages during the synthesis and analyzed them with TEM, ICP, and X-ray absorption fine structure (XAFS) spectroscopy. (Fig. 3.6, Fig. 3.7, Fig. 3.8, and Table 3.2) Until the temperature reached 220 ^{o}C, no particles were observed. At 220 ^{o}C, the solution color started to change with the nucleation. The ICP data of the sample taken at this stage showed only Pt element, and no Ni element was found. It means that only the nucleation of Pt occurred and there are Pt nanostructures in the solution. As the reaction temperature increased, Ni concentration in the nanostructures increased, indicating that the Ni metal started to be reduced. At the end of the synthesis we could get the urchin-like Pt-Ni bimetallic nanostructures whose composition was the same with the feeding ratio. The X-ray absorption near edge structure (XANES) analysis shows that the white line absorption at Pt L_{III} (E_0 = 11564 eV) edge decreased as the reaction progressed after the nucleation. It indicates that the d-band vacancies of Pt were filled, while those of Ni were

incorporated to the Pt structure to make the alloy. The extended X-ray absorption fine structure (EXAFS) results show that the Pt-M (M=Pt or Ni) coordination number decreased as the aging time increased. It can be interpreted as the growth of 1D arms in the nanostructures to form the urchin-like shapes. Recently, Wang *et al.* demonstrated the synthesis of Au-Co core-shell nanocrystals and Au-Ni spindly nanostructures by using the noble-metal-induced reduction (NMIR) process.[15] It was difficult to reduce Co^{2+} or Ni^{2+} by either octadecylamine (ODA) or Au, the coexistence of ODA and Au metal resulted in the reduction of Co^{2+} or Ni^{2+}. The formation of Pt-Ni bimetallic nanostructures in our synthetic system can be explained by the NMIR process.

The electrocatalytic activities of the urchin-like Pt-Ni nanostructures with different compositions were evaluated by using cyclic voltammetry (CV) and polarization curves, and compared with the commercial Pt/C catalyst. (Fig. 3.9) The mass activities of the urchin-like Pt_1Ni, Pt_2Ni, Pt_3Ni nanostructures and the commercial Pt catalysts at 0.9V were 0.75, 1.59, 1.34, and 0.13 A/mg_{Pt}, respectively. All the compositions of the urchin-like Pt-Ni bimetallic nanostructures show higher mass activity than the commercial Pt/C catalyst. Among them, mass ORR activity of Pt_2Ni nanostructures was the best one. It's

because of the electrochemical environment and the surface compositions of the Pt_2Ni nanostructures.[16] The urchin-like Pt_2Ni nanostructures have 12.2 times higher mass ORR activity than the commercial Pt/C, and 15.5 times higher specific ORR activity (2.94 mA/cm^2_{Pt}) than the commercial Pt/C (0.19 mA/cm^2_{Pt}).

Many previous ORR studies were conducted under $HClO_4$ conditions to exclude the effect of specific anion adsorption and to compare only the intrinsic activity of material. But in the applications of hydrogen fuel cells, the interaction between the catalysts and sulfonic acid groups in Nafion must be taken into consideration because it might block the active site of surface.[17] So we tried to measure the ORR activity in H_2SO_4 solution, and the specific activity of Pt_2Ni nanostructures (0.456 mA/cm^2_{Pt}) was 20.7 times higher than that of Pt/C (0.022 mA/cm^2_{Pt}), as shown in Fig. 3.10. To confirm the surface orientation, we conducted experiments to get the CVs of urchin-like Pt_2Ni nanostructures and the commercial Pt/C in H_2SO_4 solution under Ar atmosphere, shown in Fig. 3.11. The butterfly peak area around 0.5 V (vs. RHE) indicates that there is specific anion adsorption on the Pt (111) site.[18] The commercial Pt showed the clear butterfly peak, but in the urchin-like Pt_2Ni bimetallic nanostructures, butterfly peak didn’t appear. On the other hand, hydrogen

underpotential deposition (H_{upd}) region shows that there are (100) planes on the surface of the urchin-like Pt_2Ni nanostructures. From these results, we can estimate that the surface of the urchin-like Pt_2Ni nanostructures doesn't expose (111) planes but (100) planes dominantly. It can be explained that the specific capping agent on the (100) planes induces the slow growth of (100) planes, which results in the high coverage of (100) planes on the surface.[19] Because of the weak adsorption of sulfate anion on the (100) planes, the urchin-like Pt_2Ni nanostructures show higher performance in H_2SO_4 solution than in $HClO_4$ solution. [8(a), 18(a), 18(c)-(e), 20]

The enhanced ORR activity may be explained as two factors, the electronic and the structure effects. First, making alloy of Pt and Ni results in modifying the Pt electronic structure and altering the adsorption energy between Pt and oxygen species.[21] Fig. 3.10(c) shows the lower white line intensity of our Pt_2Ni nanostructures in Pt L_{III} XANES compared to the commercial Pt catalyst, which means that the higher occupation of the electron in 5d band in Pt_2Ni nanostructures. (L_{III} edge is electron transition from $2p_{3/2}$ to 5d orbital.) Then, the strong adsorption of OH which can act as a poisoning the active site may be reduced. The structure also affected the activity improvement. It is known that the low-coordinated sites hinder

oxygen adsorption and O-O splitting due to the strong adsorption of OH. And it can diminish the ORR activity.[22] The weak adsorption of OH on the surface of the urchin-like Pt_2Ni nanostructures is proved by the CV curve, and we can tell that on the surface of the urchin-like Pt_2Ni nanostructures, the distribution of low-coordinated site is low.[22(c)] Many 1D arms in the urchin-like Pt_2Ni nanostructures may be another factor to explain the enhanced activity. 1D morphology can improve oxygen diffusion on the surface of nanostructures.[23] Besides, the strain effect of the urchin-like dendrite structure and the high surface-to-volume ratio should be other factor to enhance the ORR activity. [13, 24, 25]

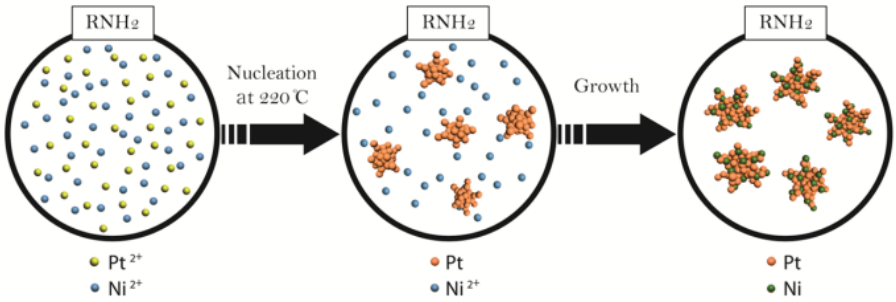

Figure 3.1 Schematic diagrams of the synthesis of urchin-like Pt-Ni bimetallic nanostructures by the NMIR process.

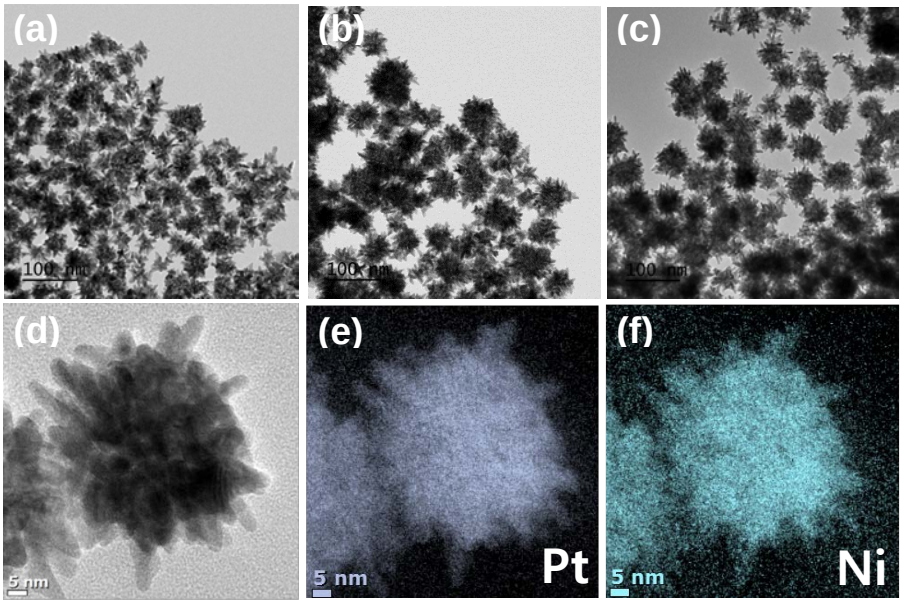

Figure 3.2 TEM images of Pt_xNi nanostructures (a) x=1, (b) x=2, (c) x=3, and (d) EF-TEM image and elemental mapping images of (e) Pt and (f) Ni element of the urchin-like Pt_2Ni nanostructures.

Table 3.1 ICP-AES data of Pt_xNi (x=1, 2, 3)

	Pt_1Ni	**Pt_2Ni**	**Pt_3Ni**
Pt : Ni	51.5 : 48.5	66.7 : 33.3	75.1 : 24.9

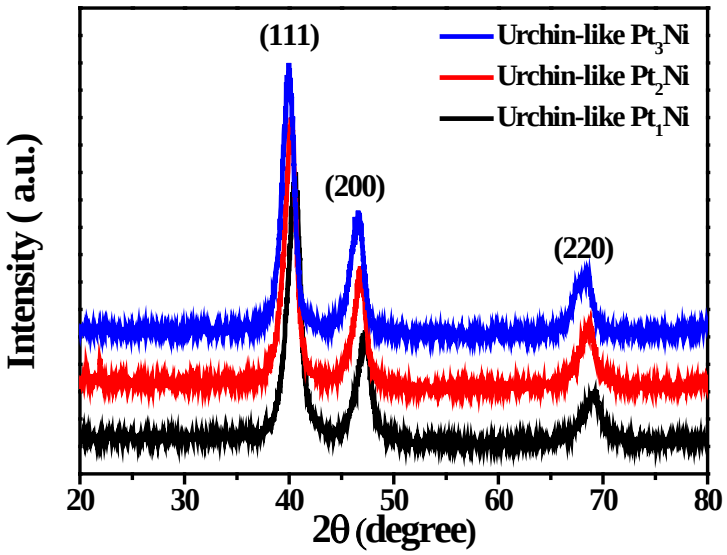

Figure 3.3 XRD patterns of the urchin-like Pt-Ni bimetallic nanostructures of three different compositions.

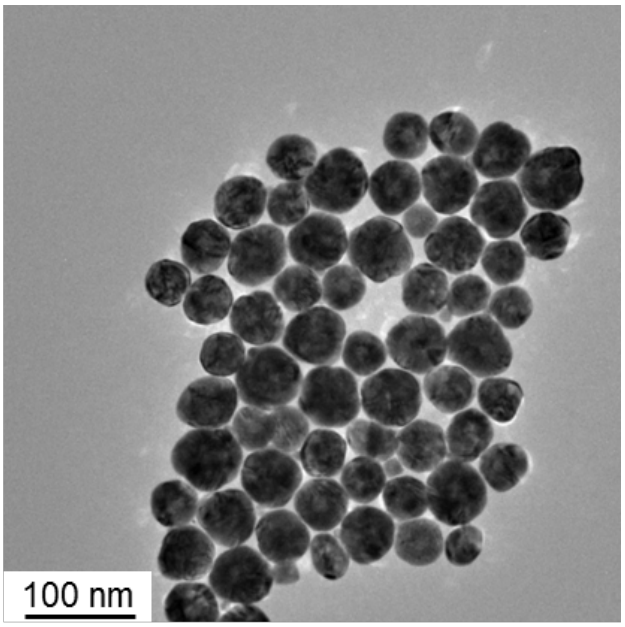

Figure 3.4 TEM image of Pt nanoparticles when only $Pt(acac)_2$ was added under the same synthesis condition.

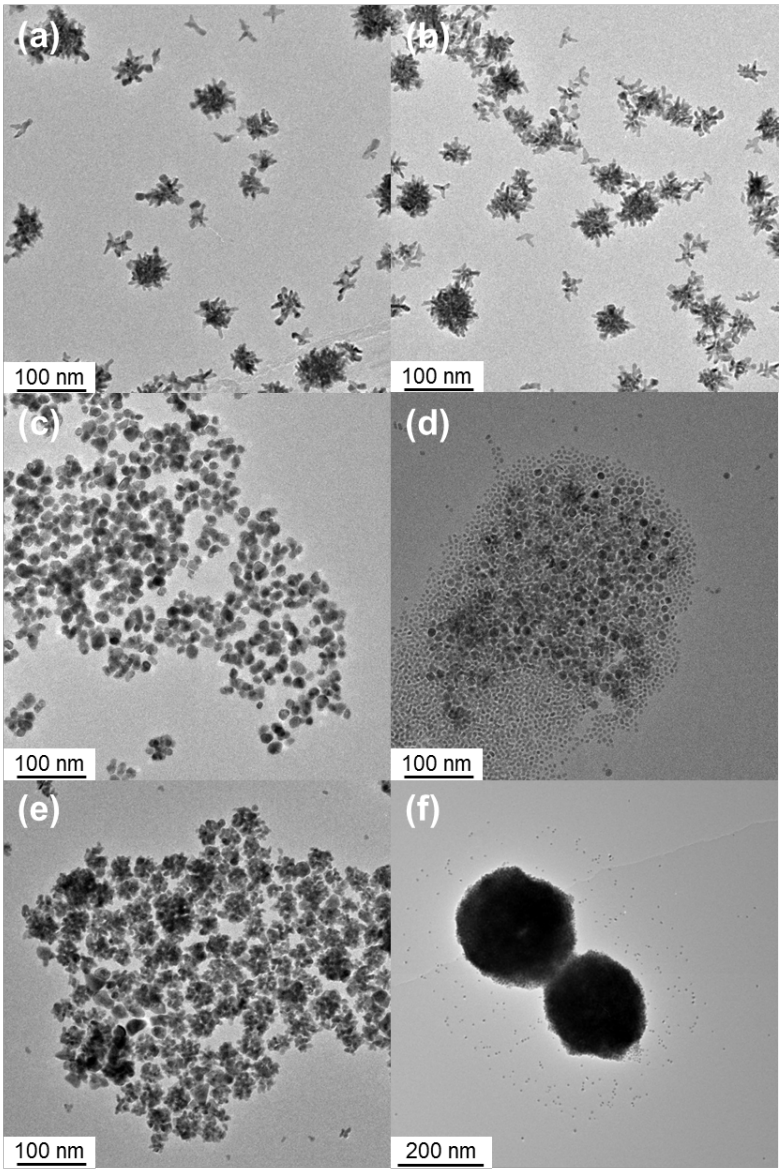

Figure 3.5 TEM images of the products synthesized at different conditions; heating rates of (a) 2 ^{o}C/min and (b)6 ^{o}C/min, reaction temperatures of (c)200 ^{o}C and (d) 260 ^{o}C, and the use of one surfactant of (e) hexadecylamine and (f) 1-adamantane carboxylic acid.

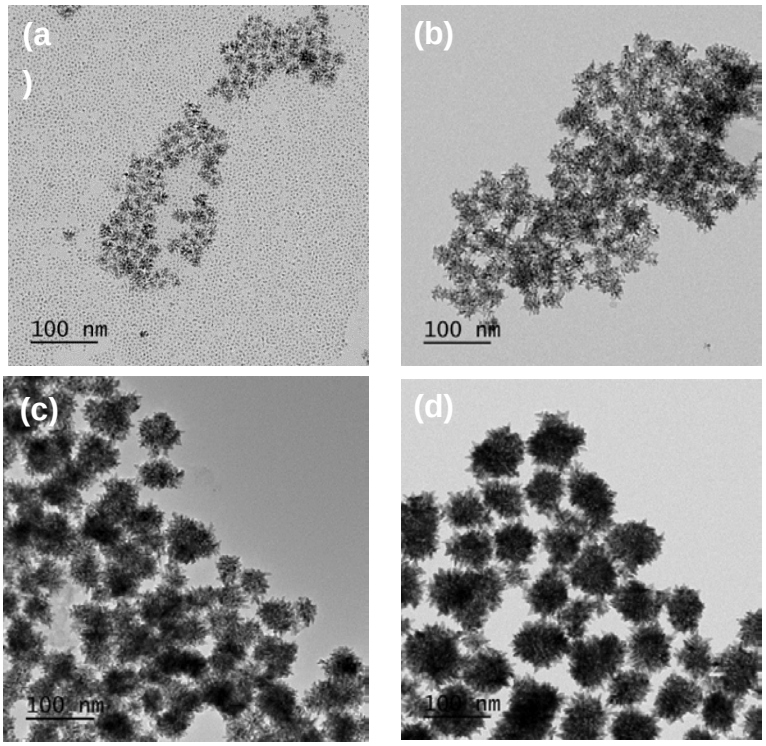

Figure 3.6 TEM images of the samples taken at the different stages of (a) 220 ºC, (b) 230 ºC, (c) 240 ºC, and (d) 240 ºC and 15 min aging.

Table 3.2 Molar ratios of Pt and Ni element of Pt_2Ni nanostructures at the different stages during the synthesis

Stage	220 °C	230 °C	240 °C 0 min	240 °C 15 min
Pt : Ni	**Only Pt**	**6.02 : 1**	**3.29 : 1**	**2.06 : 1**

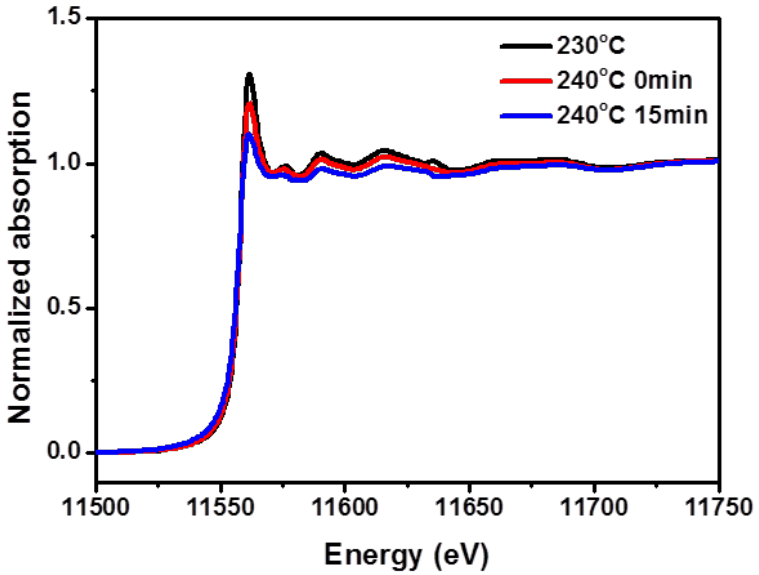

Figure 3.7 XANES spectra of Pt L_{III} edge during the synthesis of the urchin-like Pt_2Ni nanostructures.

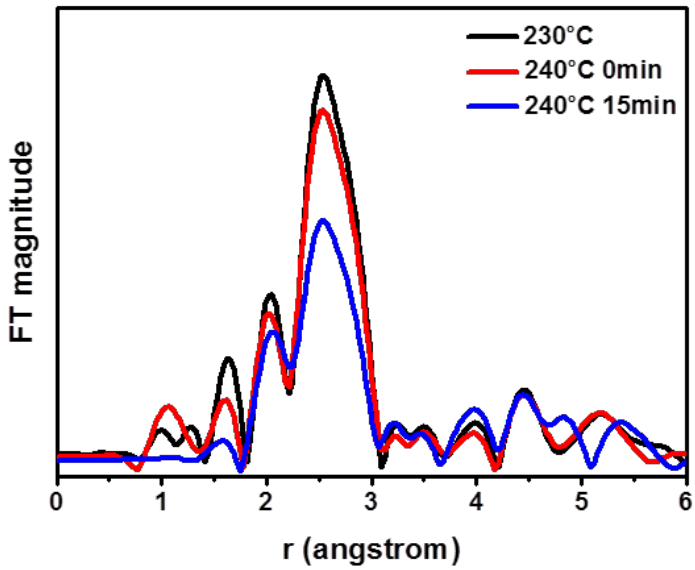

Figure 3.8 EXAFS spectra of Pt L_{III} edge during the synthesis of the urchin-like Pt_2Ni nanostructures.

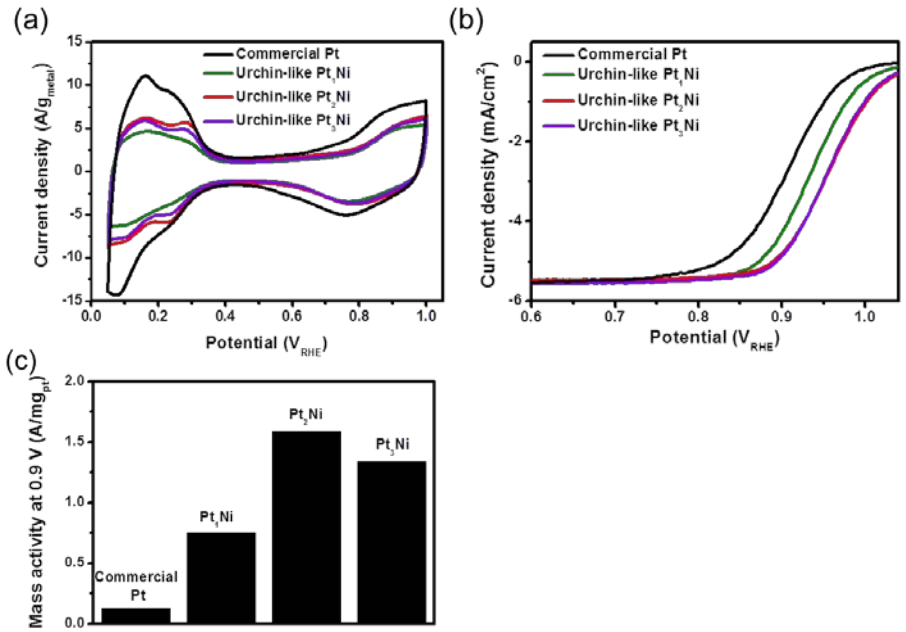

Figure 3.9 (a) Cyclic voltammograms, (b) polarization curves and (c) mass activities of the Pt_xNi nanostructures with three different compositions (x=1, 2, and 3) and the reference commercial Pt catalyst in $HClO_4$ electrolytes.

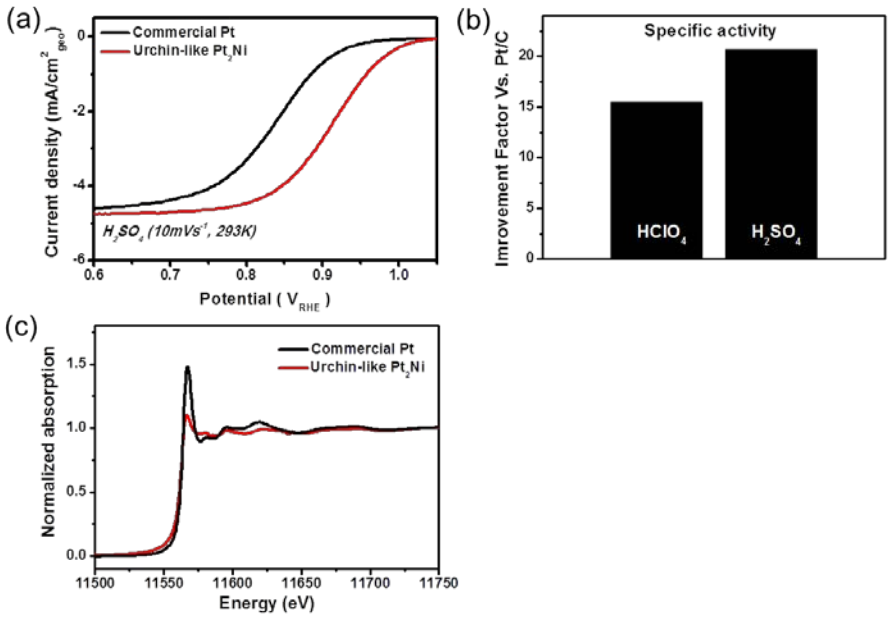

Figure 3.10 (a) Polarization curves of the urchin-like Pt_2Ni nanostructures and the commercial Pt catalysts in H_2SO_4 electrolytes, (b) improvement factors of the urchin-like Pt nanostructures in $HClO_4$ and H_2SO_4 electrolytes, and (c) Pt L_{III} XANES spectra of the urchin-like Pt_2Ni nanostructures and the commercial Pt catalyst.

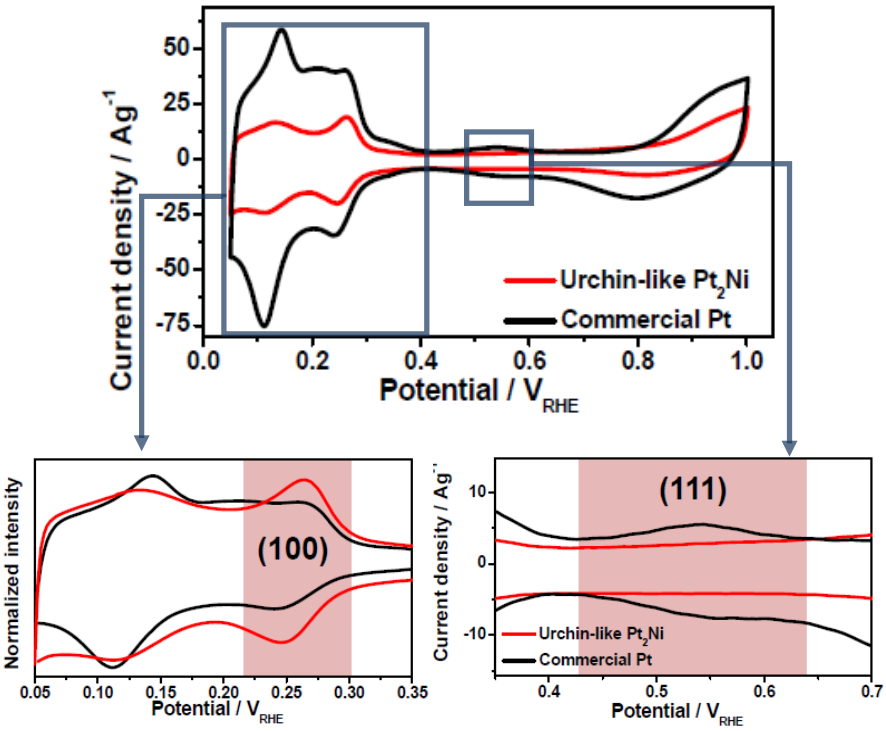

Figure 3.11 Cyclic voltammograms of the urchin-like Pt_2Ni and the commercial Pt catalyst in H_2SO_4 electrolyte.

Chapter 4 Conclusion

In conclusion, we demonstrated the simple synthesis of the urchin-like Pt-Ni nanostructures by the NMIR process. The composition of the nanostructures was controlled by varying the feeding molar ratio of $Pt(acac)_2$ and $Ni(acac)_2$. We conducted the experiments to measure ORR activity under conditions without specific anion adsorption and with specific anion adsorption. The urchin-like Pt_2Ni nanostructures showed higher activity than other urchin-like Pt-Ni nanostructures and commercial Pt catalyst. Under conditions without specific anion adsorption, Pt_2Ni nanostructures have 12.2 and 15.5 times higher mass and specific activity, respectively, than commercial Pt catalyst. While, under conditions with specific anion adsorption, our Pt_2Ni nanostructures showed 20.7 times higher than the commercial Pt catalyst.

References

1 (*a*) R. O'Hayre, S. W. Cha, W. Colella and F. B. Printz, *Fuel Cell Fundamentals*, John Wiley & Sons, New Jersey, 2006. (*b*) W. Vielstich, A. Lamm and H. A. Gasteiger, *Handbook of Fuel Cells–Fundamentals*, Technology and Applications; Wiley & Sons, U.K., 2003.

2 (*a*) EG&G Technical Services, *Fuel cell handbook 7th ed.*, Parsons Inc., 2004. (*b*) J. Zhang, *PEM Fuel Cell Electrocatalysts and Catalyst Layers: Fundamentals and Applications*, Springer, London, 2008. (*c*) K. R. Cooper, V. Ramani, J. M. Fenton and H. R. Kunz, *Experimental Methods and Data Analyses for Polymer Electrolyte Fuel Cells*, Scribner Associates Inc., North Carolina, 2005.

3 (*a*) S.-I. Choi, S. Xie, M. Shao, J. H. Odell, N. Lu, H.-C. Peng, L. Protsailo, S. Guerrero, J. Park, X. Xia, J. Wang, M. J. Kim and Y. Xia, *Nano Lett.*, 2013, **13**, 3420-3425. (*b*) J. Wu, J. Zhang, Z. Peng, S. Yang, F. T. Wagner and H. Yang, *J. Am. Chem. Soc.*, 2010, **132**, 4984-4985. (*c*) J. Wu, L. Qi, H. You, A. Gross, J. Li and H. Yang, *J. Am. Chem. Soc.*, 2012, **134**, 11880-11883.

4 J. Zhang, H. Yang, J. Fang and S. Zou, *Nano Lett.*, 2010, **10**, 638-644.

5 Grove, W. R. *Phil. Mag. Ser. 3,* 1839, **14,** 127–130 (1839).

6 Brian C. H. Steele, Angelika Heinzel, *nature* 2001, **414**, 345-352.

7 Starz, K. A., Auer, A., Lehmann, Th. & Zuber, R., *J. Power Sources* 1999, **84**, 167–172.

8 (*a*) C. Wang, H. Daimon, T. Onodera, T. Koda and S. Sun, *Angew. Chem., Int. Ed.*, 2008, **47**, 3588-3591. (*b*) V. Mazumder, Y. Lee and S. Sun, *Adv. Funct. Mater.*, 2010, **20**, 1224-1231. *(c)* J. Zhang, H. Yang, J. Fang and S. Zou, *Nano Lett.*, 2010, **10**, 638-644.

9 (*a*) V. R. Stamenkovic, B. Fowler, B. S. Mun, G. Wang, P. N. Ross, C. A. Lucas and N. M. Markovic, *Science*, 2007, **315**, 493-497. (*b*) V. R. Stamenkovic, B. S. Mun, M. Arenz, K. J. J. Mayrhofer, C. A. Lucas, G. Wang, P. N. Ross and N. M. Markovic, *Nat. Mater.*, 2007, **6**, 241-247.

10 *(a)* V. Stamenkovic, B. S. Mun, K. J. J. mayrhofer, P. N. Ross, N. M Markovic, J. Rossmeisl, J. Greeley and J. K. Nørskov, *Angew. Chem., Int. Ed*, 2006, **45**, 2897-2901. (b) J. Greeley, I. E. L. Stephens, A. S. Bondarenko, T. P. Johansson, H. A. Hansen, T. F. Jaramillo, J. Rossmeisl, I. Chorkendorff and J. K. Nørskov, *Nat. Chem.*, 2009, **1**, 552-556.

11 X. Q. Huang, E. B. Zhu, Y. Chen, Y. J. Li, C. Y. Chiu, Y. X. Xu, Z. Y. Lin, X. Duan and Y. Huang, *Adv. Mater.*, 2013, **25**, 2974-2979.

12 B. Lim, M.J. Jiang, P.H.C. Camargo, E.C. Cho, J. Tao, X.M. Lu, Y.M. Zhu, Y.A. Xia, *Science*, 2009, **324**, 1302-1305

13 D.-S. Kim, C. Kim, J.-K. Kim, J.-H. Kim, H.-H. Chun, H. Lee and Y.-T. Kim, *J. Catal.*, 2012, **291**, 69-78.

14 (*a*) Y. Yin and A. P. Alivisatos, *Nature*, 2005, **437**, 664-670. (*b*) E. V. Shevchenko, D. V. Talapin, A. L. Rogach, A. Kornowski, M. Haase, and H. Weller, *J. Am. Chem. Soc.*, 2002, **124**, 11480-11485. (*c*) T, Mokari, M. J. Zhang and P. D. Yang, *J. Am. Chem. Soc.*, 2007, **129**, 9864-9865. (*d*) A. R. Tao, S. Habas and P. D. Yang, *Small*, 2008, **4**, 310-325. (*e*) S.-W. Chou, C.-L. Zhu, S. Neeleshwar, C.-L. Chen, Y.-Y. Chen and C.-C. Chen, *Chem. Mater.*, 2009, **21**, 4955-4961. (*f*) Z. Peng and H. Yang, *Nano Today*, 2009, **4**, 143-164. (*g*) S. Cheong, J. D. Watt and R. D. Tilley, *Nanoscale*, 2010, **2**, 2045-2053.

15 D. S. Wang and Y. D. Li, *J. Am. Chem. Soc.*, 2010, **132**, 6280-6281.

16 (*a*) C. Wang, M. Chi, G. Wang, D. van der Vliet, D. Li, K. More, H.-H. Wang, J. A. Schlueter, N. M. Markovic and V. R.

Stamenkovic, *Adv. Funct. Mater.*, 2011, **21**, 147-152. (*b*) Y. H. Chung, D. Y. Chung, N. Jung, H. Y. Park, Y.-E. Sung and S. J. Yoo, *Int. J. Hydrogen Energy*, 2014, **39**, 14751-14759.

17 (*a*) M. Teliska, V. S. Murthi, S. Mukerjee and D. E. Ramaker, *J. Phys. Chem. C*, 2007, **111**, 9267-9274. (*b*) R. Subbaraman, D. Strmcnik, V. Stamenkovic and N. M. Markovic, *J. Phys. Chem. C*, 2010, **114**, 8414-8422. (*c*) R. Subbaraman, D. Strmcnik, A. P. Paulikas, V. R. Stamenkovic and N. M. Markovic, *ChemPhysChem*, 2010, **11**, 2825-2833. (*d*) Y.-H. Chung, S. J. Kim, D. Y. Chung, M. J. Lee, J. H. Jang and Y.-E. Sung, *Phys. Chem. Chem. Phys.*, 2014, **16**, 13726-13732.

18 (*a*) N. M. Markovic, H. A. Gasteiger and P. N. Ross, *J. Phys. Chem.*, 1995, **99**, 3411-3415. (*b*) J. Mostany, E. Herrero, J. M. Feliu and J. Lipkowski, *J. Phys. Chem. B*, 2002, **106**, 12787-12796. (*c*) C. M. Sánchez-Sánchez, J. Solla-Gullón, F. J. Vidal-Iglesias, A. Aldaz, V. Montiel and E. Herrero, *J. Am. Chem. Soc.*, 2010, **132**, 5622-5624. (*d*) Q. S. Chen, F. J. Vidal-Iglesias, J. Solla-Gullón, S. G. Sun and J. M. Feliu, *Chem. Sci.*, 2012, **3**, 136-147. (*e*) C. Wang, H. Daimon, Y. Lee, J. Kim and S. Sun, *J. Am. Chem. Soc.*, 2007, **129**, 6974-6975.

19 (*a*) Y.-W. Jun, J.-S. Choi and J. Cheon, *Angew. Chem., Int. Ed.*, 2006, **45**, 3414-3439. (*b*) X. H. Xia, J. Zeng, L. K. Oetjen, Q. Li and Y. N. Xia, *J. Am. Chem. Soc.*, 2012, **134**, 1793-1801. (*c*) C. R. Bealing, W. J. Baumgardner, J. J. Choi, T. Hanrath and R. G. Hennig, *ACS Nano*, 2012, **6**, 2118-2127.

20 (*a*) D. Armand and J. Clavilier, *J. Electroanal. Chem.*, 1989, **263**, 109-126. (*b*) D. Armand and J. Clavilier, *J. Electroanal. Chem.*, 1989, **270**, 331-347. (*c*) N. Markovic, H. Gasteiger and P. N. Ross, *J. Electrochem. Soc.*, 1997, **144**, 1591-1597.

21 (*a*) Y. S. Kim, S. H. Jeon, A. Bostwick, E. Rotenberg, P. N. Ross, V. R. Stamenkovic, N. M. Markovic, T. W. Noh, S. Han and B. S. Mun, *Adv. Energy Mater.*, 2013, **3**, 1257-1261. (*b*) S. J. Hwang, S. K. Kim, J. G. Lee, S. C. Lee, J. H. Jang, P. Kim, T. H. Lim, Y.-E. Sung and S. J. Yoo, *J. Am. Chem. Soc.*, 2012, **134**, 19508-19511.

22 (*a*) K. J. J. Mayrhofer, B. B. Blizanac, M. Arenz, V. R. Stamenkovic, P. N. Ross and N. M. Markovic *J. Phys. Chem. B*, 2005, **109**, 14433-14440. (*b*) J. L. Zhang, M. B. Vukmirovic, Y. Xu, M. Mavrikakis and R. R. Adzic, *Angew. Chem., Int. Ed.*, 2005, **44**, 2132-2135. (*c*) Y. Cai, C. Ma, Y. Zhu, J. X. Wang and R. R. Adzic, *Langmuir*, 2011, **27**, 8540-8547.

23 S. Sun, G. Zhang, Y. Geng, Y. Chen, R. Li, M. Cai and X. Sun, *Angew. Chem., Int. Ed.*, 2011, **50**, 422-426.

24 J. Wu, L. Qi, H. You, A. Gross, J. Li and H. Yang, *J. Am. Chem. Soc.*, 2012, **134**, 11880-11883.

25 P. Strasser, S. Koh, T. Anniyev, J. Greeley, K. More, C. Yu, C. Z. Liu, S. Kaya, D. Nordlund, H. Ogasawara, M. F. Toney and A. Nilsson, *Nat. Chem.*, 2010, **2**, 454-460.

초록

수소이온 교환막 연료전지(proton exchange membrane fuel cell, PEMFC)는 환경 친화적인 에너지 기술로 촉망받고 있다. 이 PEMFC 에서 가장 중요한 반응은 환원전극에서의 산소환원 반응(oxygen reduction reaction, ORR)이다. 현재 ORR 에 사용되는 전기화학촉매인 Pt 는 가격이 비싸고 매장량이 적은 것이 문제점으로 지적되고 있다. ORR 은 전체 반응 중 가장 느리기 때문에 전체 반응속도를 결정하므로 ORR 촉매 개발은 PEMFC 의 산업화를 위해서 반드시 필요하다. ORR 에 사용되는 전기화학촉매에 대한 많은 연구 보고가 있는데, 그 중 Pt 와 Ni 의 합금이 Pt 의 사용량도 줄일 수 있고, 상용 Pt 보다 활성이 높기 때문에 가장 유력한 후보물질 중 하나로 고려되고 있다. 그래서 많은 연구진들이 더 높은 활성을 위해 표면적이 넓은 Pt-Ni 나노물질을 ORR 전기화학촉매로 사용한 보고들이 있다. 하지만 합성을 정교하게 컨트롤하기가 어렵다는 문제점이 있다. 여기서 우리는, ORR 전기화학 촉매로 사용하기 위해 성게 모양의 Pt-Ni 나노구조를 간단한 heat-up 방법으로 합성했다.

합금 조성은 전구체의 몰 비율로 조절했다. 그 결과로 합성된 성게모양의 Pt-Ni 나노구조는 상용 Pt 촉매보다 높은 활성을 나타냈다.

주요어 : 산소환원반응, 수소이온 교환막 연료전지, 성게 모양 나노구조, 전기화학촉매, Pt-Ni 합금

학번 : 2012-23266